DOI 10.1007/s10946-023-10114-0
Journal of Russian Laser Research, Volume 44, Number 1, January, 2023

PROPAGATION CHARACTERISTICS OF PARTIALLY-COHERENT RADIALLY-POLARIZED VORTEX BEAMS THROUGH NON-KOLMOGOROV TURBULENCE ALONG A SLANT PATH

Kai Huang,[1,2] Yonggen Xu,[3*] Jin Cao,[1,2] and Yuqiang Li[4]

[1] *College of Mathematics and Physics, Leshan Normal University Leshan 614000, China*

[2] *Key Laboratory of Detection and Application of Space Effect in Southwest Sichuan Leshan Normal University Leshan 614000, China*

[3] *Department of Physics, School of Science, Xihua University Chengdu 610039, China*

[4] *Group of Applied Astronomy Research, Yunnan Observatory, Chinese Academy of Sciences Kunming 650011, China*

*Corresponding author e-mail: xuyonggen06 @ 126.com

Abstract

We explore the propagation characteristics of a partially-coherent radially-polarized vortex beam (PCRPVB) with Gaussian Schell-model correlation structure and, using the extended Huygens–Fresnel principle, derive analytical formulas for the average intensity of PCRPVB propagating through the non-Kolmogorov atmospheric turbulence along a slant path. Numerical results show that the normalized initial profile with a hollow distribution of PCRPVB in turbulence gradually converts into a flat-topped distribution with increasing propagation distance and zenith angle, and finally evolves into a Gaussian-like profile. Also, we can find that a PCRPVB with the high topological charges l has the stronger ability of resisting turbulence in comparison with the non-vortex beam. Our work will be useful for free-space optical communications, remote sensing, and the lidar distance measurement.

Keywords: PCRPVB, non-Kolmogorov atmospheric turbulence, normalized average intensity, zenith angle, topological charge.

1. Introduction

It is well known that the optical vortex with an azimuthal phase $\exp(il\varphi)$ may have an orbital angular momentum (OAM) $l\hbar$ per photon due to the undetermined phase, where l is the topological charge, φ denotes the azimuthal angle, and $\hbar$ is Planck's constant h divided by 2π [1–16]. Over the past decades, a great deal of attention has been paid to light beams carrying OAM due to the such important applications as free space optical communications [3–9], optical manipulation [4, 5], and quantum cryptography and quantum information processing [6–16]. Partially coherent (PC) beams display many extraordinary behaviors and are useful in many areas because of its lower coherence and stronger propagation stability than the fully coherent beams, such as inertial confinement fusion, lithography, optical imaging, remote

Manuscript submitted by the authors in English on November 24, 2022.

1071-2836/23/4401-0110

sensing and the lidar distance measurement [14,17–21]. On the other hand, polarization is one of the most salient features of a laser beam, which indicates the oscillation state of electric field at a spatial point. The radially polarized (RP) beams, whose state of polarization is linearly polarized but its oscillation direction at any point is along the radial direction, have attracted wide attention due to its unique tight focusing properties; they have important applications in plasmonic focusing, material processing, second-harmonic generation, particle trapping, and detection [14–25]. Furthermore, it was shown that the radially-polarized partially-coherent (RPPC) beam with vortex phase can effectively reduce the effect of atmospheric turbulence [20,21,23]; therefore, the beams with the especial structure are attracted more and more attention.

The atmospheric turbulence causes many harmful turbulence effects, such as light intensity scintillation, phase distortion, which results in increase of communication error rate and reduces the channel capacity of the system. On the other hand, the atmospheric turbulence is usually assumed to be homogeneous. However, the researches show that the structure parameter of the refractive index fluctuations of the atmospheric turbulence drops gradually as the propagation height increase for a slant path [26–35]. Up to our knowledge, till now the propagation characteristics of partially-coherent radially-polarized vortex beam (PCRPVB) passing through non-Kolmogorov turbulence along a slant path have not been reported due to the difficulties in mathematical calculations. Therefore, in this paper, our aim is to explore the average intensity of PCRPVB in turbulence along a slant path. Our numerical results imply that a PCRPVB with the high topological charges l has the stronger ability of resisting turbulence in comparison with the non-vortex beam.

2. Theoretical Model

The electric filed of a fully-coherent radially-polarized vortex beam (FCRPVB) reads [14–16]

$$\boldsymbol{E}(\boldsymbol{\rho}';0)=\frac{x}{w_0}\exp\left(-\frac{\rho'^{\,2}}{w_0^2}\right)\left(\frac{\rho'^{\,2}}{w_0^2}\right)^{|l|/2}\exp(il\theta')e_x+\frac{y}{w_0}\exp\left(-\frac{\rho'^{\,2}}{w_0^2}\right)\left(\frac{\rho'^{\,2}}{w_0^2}\right)^{|l|/2}\exp(il\theta')\boldsymbol{e}_y, \tag{1}$$

where the vector $\boldsymbol{\rho}'=(x,y)$ is arbitrary transverse position vector in the plane $z=0$, w_0 represents the waist radius of a fundamental Gaussian beam, $\boldsymbol{e}_x$ and $\boldsymbol{e}_y$ denote the unit vectors in the x and y directions, respectively, and $\exp(il\theta')$ terms represent the topological charge and the azimuthal coordinate, with l and $\theta'=\arctan(y/x)$, respectively.

For the PC beam, the statistical properties of a PCRPVB with Gaussian Schell-model correlation structure are characterized by a 2×2 cross-spectral density matrix (CSDM). The elements of CSDM of PCRPVB in the initial plane $z=0$ are given by

$$\begin{aligned} W_{uv}(\boldsymbol{\rho}_1',\boldsymbol{\rho}_2';0) &= \frac{u_1v_2}{w_0^2}\exp\left(-\frac{\rho_1'^2+\rho_2'^2}{w_0^2}\right)\left(\frac{\rho_1'^2\rho_2'^2}{w_0^4}\right)^{|l|/2}\exp[-il(\theta_1'-\theta_2')]\exp\left[-\frac{|\rho_1'-\rho_2'|^2}{2\delta_{uv}^2}\right]; \\ u,v &= x,y, \end{aligned} \tag{2}$$

where $\boldsymbol{\rho}_1'=(x_1,y_1)$ and $\boldsymbol{\rho}_2'=(x_2,y_2)$ are the arbitrary transverse position vectors in the initial plane ($z=0$), δ_{uv} represent the initial auto-correlation lengths (when $u=v$) and the initial mutual correlation lengths (when $u\neq v$), respectively. In this paper, we set $\delta_{xx}=\delta_{yy}=\delta_{xy}=\delta_{yx}=\delta_0$.

We know that the expression of general vortex beam can be derived from the degradation of Laguerre–Gaussian (LG) vortex beam. Besides, the LG mode can be represented by the Hermite-Gaussian (HG) modes as follows [20–23]:

$$\exp(il\theta')r^l L_p^l(\rho'^2) = \frac{(-1)^p}{2^{2p+l}p!}\sum_{t=0}^{p}\sum_{s=0}^{l} i^s \begin{pmatrix} p \\ t \end{pmatrix}\begin{pmatrix} l \\ s \end{pmatrix} H_{2t+l-s}(x)H_{2p-2t+s}(y), \tag{3}$$

where $H_{2t+l-s}(x)$ and $H_{2p-2t+s}(y)$ are the Hermite polynomials, and (p,t) and (l,s) represent the binomial coefficients. So, after substituting Eq. (3) into Eq. (2), with setting $p=0$, we arrive at the expression of CSDM of PCRPVB in the form with Hermite–Gaussian mode; it reads

$$\begin{aligned} W_{uv}(\boldsymbol{\rho}_1', \boldsymbol{\rho}_2'; 0) = {} & \frac{u_1 v_2}{w_0^2}\exp\left(-\frac{\rho_1'^2+\rho_2'^2}{w_0^2}\right)\exp\left[-\frac{|\boldsymbol{\rho}_1'-\boldsymbol{\rho}_2'|^2}{2\delta_{uv}^2}\right]\frac{1}{2^{2m}}\sum_{s=0}^{l}\sum_{\nu=0}^{l}(i^s)^* i^v \\ & \times \begin{pmatrix} m \\ s \end{pmatrix}\begin{pmatrix} m \\ \nu \end{pmatrix} H_{l-s}\left(\frac{x_1}{w_0}\right) H_{l-\nu}\left(\frac{x_2}{w_0}\right) H_s\left(\frac{y_1}{w_0}\right) H_\nu\left(\frac{y_2}{w_0}\right). \end{aligned} \tag{4}$$

Using the extended Huygens–Fresnel principle, we can express the CSDM of beams through atmospheric turbulence in the received plane as follows [30–38]:

$$\begin{aligned} W_{uv}(\boldsymbol{\rho}_1, \boldsymbol{\rho}_2; z) = {} & \left(\frac{k}{2\pi z}\right)^2 \iiiint W_{uv}(\rho_1', \rho_2'; 0) \\ & \times \exp\left[-\frac{ik(\boldsymbol{\rho}_1-\boldsymbol{\rho}_1')^2}{2z} + \frac{ik(\boldsymbol{\rho}_2-\boldsymbol{\rho}_2')^2}{2z} - \frac{D_w(\boldsymbol{\rho}_1', \boldsymbol{\rho}_2', \boldsymbol{\rho}_1, \boldsymbol{\rho_2}; z)}{2}\right] d^2\rho_1' d^2\rho_2', \end{aligned} \tag{5}$$

where $\boldsymbol{\rho}_1 = (\rho_{x1}, \rho_{y1})$ and $\boldsymbol{\rho}_2 = (\rho_{x2}, \rho_{y2})$ denote two arbitrary transverse position vectors in the received plane, $k = 2\pi/\lambda$ is the wave number, with λ being the wavelength, and $D_w(\boldsymbol{\rho}_1', \boldsymbol{\rho}_2', \boldsymbol{\rho}_1, \boldsymbol{\rho}_2; z)$ is a two-point spherical wave structure function containing the influence of atmospheric turbulence; its expression is [26–30]

$$D_w(\boldsymbol{\rho}_1', \boldsymbol{\rho}_2', \boldsymbol{\rho}_1, \boldsymbol{\rho}_2; z) = \frac{8\pi^2 k^2}{\cos(\gamma)}\int_{h_0}^{H} dh \int_0^\infty \left\{1 - J_0\left[\varkappa\left|\zeta(\boldsymbol{\rho}_1'-\boldsymbol{\rho}_2') + (1-\zeta)(\boldsymbol{\rho}_1-\boldsymbol{\rho}_2)\right|\right]\right\}\Phi_n(\varkappa, h)\varkappa\, d\varkappa, \tag{6}$$

where $J_0(\cdot)$ is the zero-order Bessel function of the first kind, $\Phi_n(\varkappa, h)$ represents the spatial power spectrum of the refractive-index fluctuations of atmospheric turbulence, with $\varkappa$ denoting the spatial wavenumber. Also, H is the height between the received plane and the ground, and h_0 is the height between the light source plane and the ground, when the beams are propagating in atmospheric turbulence along a slant path, and $\zeta = 1-(h-h_0)/[z\cos(\gamma)]$ denotes the normalized distance variable, with γ being the zenith angle and $z = (H-h_0)/\cos(\gamma)$ being the total propagation distance along a slant path. Generally, we take $h_0 = 0$, which means that the light source plane is on the ground.

In this paper, we use the non-Kolmogorov power spectrum as a model for atmospheric turbulence,

and its spatial power spectrum $\Phi_n(\varkappa, h)$ is given by [26–35]:

$$\Phi_n(\varkappa, h) = \tilde{C}_n^2(h)\frac{A(\alpha)}{(\varkappa^2 + \varkappa_0^2)^{\alpha/2}} \exp\left(-\frac{\varkappa^2}{\varkappa_m^2}\right) = \tilde{C}_n^2(h)\Phi_n'(\varkappa), \tag{7}$$

$$A(\alpha) = \frac{1}{4\pi^2}\Gamma(\alpha - 1)\cos(\alpha\pi/2), \tag{8}$$

$$c(\alpha) = \left[\frac{2\pi}{3}A(\alpha)\Gamma\left(\frac{5-\alpha}{2}\right)\right]^{1/(\alpha-5)}, \tag{9}$$

where $\varkappa_0 = 2\pi/L_0$ with L_0 being the outer scale of atmospheric turbulence, and $\varkappa_m = c(\alpha)/l_0$ with l_0 being the inner scale of atmospheric turbulence. Also, α is the generalized exponent parameter, $\Gamma(\cdot)$ is the gamma function, and $\tilde{C}_n^2(h)$ is the generalized refractive-index structure parameter varying with height h. The Hufnagel–Valley atmospheric turbulence profile model (H-V5/7 model) is generally used for the propagation along a slant path [30–35],

$$C_n^2(h) = 0.00594\left(\frac{V_s}{27}\right)^2 (10^{-5}h)^{10}\exp\left(\frac{-h}{1000}\right) + 2.7\cdot 10^{-16}\exp\left(\frac{-h}{1500}\right) + 1.7\cdot 10^{-14}\exp\left(\frac{-h}{100}\right), \tag{10}$$

where V_s represents the wind speed, which is usually taken as 21 m/s.

Considering the quadratic approximation of the Rytov phase structure function in Eq. (6), we can rewrite Eq. (6) as follows:

$$D_w(\boldsymbol{\rho}_1', \boldsymbol{\rho}_2', \boldsymbol{\rho}_1, \boldsymbol{\rho}_2; z) \approx B_1(\boldsymbol{\rho}_1 - \boldsymbol{\rho}_2)^2 + B_2(\boldsymbol{\rho}_1 - \boldsymbol{\rho}_2)\cdot(\boldsymbol{\rho}_1' - \boldsymbol{\rho}_2') + B_3(\boldsymbol{\rho}_1' - \boldsymbol{\rho}_2')^2, \tag{11}$$

with

$$B_1 = \frac{2\pi^2 k^2}{\cos\gamma} T\int_{h_0}^{H}(1-\zeta)^2 C_n^2(h)\, dh, \tag{12}$$

$$B_2 = \frac{2\pi^2 k^2}{\cos\gamma} T\int_{h_0}^{H}2(1-\zeta)\zeta C_n^2(h)\, dh, \tag{13}$$

$$B_3 = \frac{2\pi^2 k^2}{\cos\gamma} T\int_{h_0}^{H}\zeta^2 C_n^2(h)\, dh, \tag{14}$$

$$T = \int_0^\infty \varkappa^3\Phi_n'(\varkappa)\, d\varkappa, \tag{15}$$

where T denotes the intensity of the turbulent atmosphere, which can only be determined by the spatial power spectrum, and is independent of the beam parameters [36–38].

After substituting Eqs. (7)–(9) into Eq. (15), we arrive at

$$T = \frac{A(\alpha)}{2(\alpha-2)}\left\{\left[2\varkappa_0^2\varkappa_m^{2-\alpha} + (\alpha-2)\varkappa_m^{4-\alpha}\right]\exp\left(\frac{\varkappa_0^2}{\varkappa_m^2}\right)\Gamma\left(2-\frac{\alpha}{2}, \frac{\varkappa_0^2}{\varkappa_m^2}\right) - 2\varkappa_0^{4-\alpha}\right\}, \tag{16}$$

where $\Gamma(\cdot,\cdot)$ is an incomplete gamma function. Setting $\boldsymbol{\rho}_1 = \boldsymbol{\rho}_2 = \boldsymbol{\rho}$, we can simplify Eq. (5) to the following one:

$$\begin{aligned} W_{uv}(\boldsymbol{\rho}, \boldsymbol{\rho}; z) &= \left(\frac{k}{2\pi z}\right)^2 \iiint W_{uv}(\boldsymbol{\rho}_1', \boldsymbol{\rho}_2'; 0) \\ &\times \exp\left[-\frac{ik(\boldsymbol{\rho} - \boldsymbol{\rho}_1')^2}{2z} + \frac{ik(\boldsymbol{\rho} - \boldsymbol{\rho}_2')^2}{2z} - \frac{B_3(\boldsymbol{\rho}_1' - \boldsymbol{\rho}_2')^2}{2}\right] d^2\boldsymbol{\rho}_1'\, d^2\boldsymbol{\rho}_2' \end{aligned} \tag{17}$$

and obtain the analytical formulas for the $W_{xx}(\boldsymbol{\rho},\boldsymbol{\rho};z)$ and $W_{yy}(\boldsymbol{\rho},\boldsymbol{\rho};z)$ of the PCRPVB through the turbulent atmosphere along a slant path; they are

$$
\begin{aligned}
W_{xx}(\boldsymbol{\rho},\boldsymbol{\rho};z) &= \left(\frac{k}{2zw_0}\right)^2 \exp\left(\frac{C_{1x}^2}{4A}\right)\exp\left(\frac{E^2}{4D}\right)\exp\left(\frac{C_{1y}^2}{4A}\right)\exp\left(\frac{F^2}{4D}\right)\frac{1}{2^{2m}} \\
&\times \sum_{s=0}^{l}\sum_{\nu=0}^{l}(i^s)^* i^\nu \begin{pmatrix} l \\ s \end{pmatrix}\begin{pmatrix} l \\ \nu \end{pmatrix} \sum_{a_1=0}^{[(l-s)/2]} \sum_{a_2=0}^{l-s-2a_1+1} \sum_{a_3=0}^{[a_2/2]} \sum_{a_4=0}^{[(l-\nu)/2]} \sum_{a_5=0}^{s} \sum_{a_6=0}^{[a_5/2]} \sum_{a_7=0}^{[\nu/2]} \begin{pmatrix} l-s-2a_1+1 \\ a_2 \end{pmatrix}\begin{pmatrix} s \\ a_5 \end{pmatrix} \\
&\times \frac{(i)^{-2l+s+4a_1+2a_3+4a_4-a_5+4a_6+4a_7-2} a_2!a_5!(l-s)!(l-\nu)!\nu!}{a_1!a_3!a_4!a_6!a_7!(a_2-2a_3)!(a_5-2a_6)!(l-s-2a_1)!(l-\nu-2a_4)!(\nu-2a_7)!} \\
&\times 2^{(-l+2a_1-a_2+2a_3-a_5+2a_6-5)/2}\left(\frac{1}{w_0}\right)^{2l-2a_1-2a_4-2a_7}\left(\frac{1}{\sqrt{A}}\right)^{l+s-2a_1+a_2-2a_3+3}\left(\frac{1}{\sqrt{A^2w_0^2-A}}\right)^{-s+a_5-2a_6} \\
&\times (B)^{a_2-2a_3+a_5-2a_6}\left(\frac{1}{\sqrt{D}}\right)^{l+a_2-2a_3-2a_4+a_5-2a_6-2a_7+3} H_{l-s-2a_1+1-a_2}\left(\frac{\sqrt{2}iC_{1x}}{2\sqrt{A}}\right) \\
&\times H_{l-\nu+a_2-2a_3-2a_4+1}\left(\frac{iE}{2\sqrt{D}}\right) H_{s-a_5}\left(\frac{\sqrt{2}C_{1y}}{2\sqrt{A^2w_0^2-A}}\right) H_{\nu+a_5-2a_6-2a_7}\left(\frac{iF}{2\sqrt{D}}\right), \quad (18)
\end{aligned}
$$

and

$$
\begin{aligned}
W_{yy}(\boldsymbol{\rho},\boldsymbol{\rho};z) &= \left(\frac{k}{2zw_0}\right)^2 \exp\left(\frac{C_{1x}^2}{4A}\right)\exp\left(\frac{E^2}{4D}\right)\exp\left(\frac{C_{1y}^2}{4A}\right)\exp\left(\frac{F^2}{4D}\right)\frac{1}{2^{2m}} \\
&\times \sum_{s=0}^{l}\sum_{\nu=0}^{l}(i^s)^* i^\nu \begin{pmatrix} l \\ s \end{pmatrix}\begin{pmatrix} l \\ \nu \end{pmatrix} \sum_{a_1=0}^{l-s} \sum_{a_2=0}^{[a_1/2]} \sum_{a_3=0}^{[(l-\nu)/2]} \sum_{a_4=0}^{[s/22]} \sum_{a_5=0}^{s-2a_4+1} \sum_{a_6=0}^{[a_5/2]} \sum_{a_7=0}^{[\nu/2]} \begin{pmatrix} l-s \\ a_1 \end{pmatrix}\begin{pmatrix} s-2a_4+1 \\ a_5 \end{pmatrix} \\
&\times \frac{(i)^{-l-s-a_1+4a_2+4a_3+4a_4+2a_6+4a_7-2} a_1!a_5!(l-\nu)!s!\nu!}{a_2!a_3!a_4!a_6!a_7!(a_1-2a_2)!(a_5-2a_6)!(l-\nu-2a_3)!(s-2a_4)!(\nu-2a_7)!} \\
&\times 2^{(-l-a_1+2a_2+2a_4-a_5+2a_6-5)/2}\left(\frac{1}{w_0}\right)^{2l-2a_3-2a_4-2a_7}\left(\frac{1}{\sqrt{A}}\right)^{2l-s-2a_4+a_5-2a_6+3}\left(\frac{1}{\sqrt{A^2w_0^2-A}}\right)^{-l+s+a_1-2a_2} \\
&\times (B)^{a_1-2a_2+a_5-2a_6}\left(\frac{1}{\sqrt{D}}\right)^{l+a_1-2a_2-2a_3+a_5-2a_6-2a_7+3} H_{l-s-a_1}\left(\frac{\sqrt{2}C_{1x}}{2\sqrt{A^2w_0^2-A}}\right) \\
&\times H_{l-\nu+a_1-2a_2-2a_3}\left(\frac{iE}{2\sqrt{D}}\right) H_{s-2a_4-a_5+1}\left(\frac{\sqrt{2}iC_{1y}}{2\sqrt{A}}\right) H_{\nu+a_5-2a_6-2a_7+1}\left(\frac{iF}{2\sqrt{D}}\right), \quad (19)
\end{aligned}
$$

where

$$
\begin{gathered}
A = \frac{1}{w_0^2}+\frac{1}{2\delta_0^2}+\frac{ik}{2z}+\frac{B_3}{2}, \qquad B = \frac{1}{\delta_0^2}+B_3, \qquad C_{1x} = \frac{ik\rho_x}{z}, \qquad C_{1y} = \frac{ik\rho_y}{z}, \\
C_{2x} = -\frac{ik\rho_x}{z}, \quad C_{2y} = -\frac{ik\rho_y}{z}, \quad D = -\frac{B^2}{4A}+A^*, \quad E = \frac{BC_{1x}}{2A}+C_{2x}, \quad F = \frac{BC_{1y}}{2A}+C_{2y}
\end{gathered} \quad (20)
$$

and

$$B_3 = T\left\{\frac{\pi^2k^2V_s^2}{z\cos\gamma}\exp\left(\frac{-z\cos\gamma}{1000}\right)\left[-1.1827\cdot10^{-42}\sum_{n=1}^{9}\frac{n(n+1)}{(11-n)!}(z\cos\gamma)^{9-n}10^{3n}-\frac{1.301\cdot10^{-10}}{z\cos\gamma}\right]\right.$$
$$+\frac{\pi^2k^2}{z^3\cos^3\gamma}\left[-1.5612\cdot10^{-7}\exp\left(\frac{-z\cos\gamma}{1000}\right)V_s^2-7.2902\cdot10^{-6}\exp\left(\frac{-z\cos\gamma}{1500}\right)\right]$$
$$+\frac{\pi^2k^2}{z^3\cos^3\gamma}\left[-1.36\cdot10^{-7}\exp\left(\frac{-z\cos\gamma}{100}\right)+1.5612\cdot10^{-7}V_s^2+7.4262\cdot10^{-6}\right]$$
$$\left.+\frac{\pi^2k^2}{z^2\cos^2\gamma}\left(-2.602\cdot10^{-11}V_s^2-6.22\cdot10^{-9}\right)+\frac{\pi^2k^2}{z\cos\gamma}\cdot8.4201\cdot10^{-12}\right\}. \tag{21}$$

The average intensity of PCRPVB through atmospheric turbulence along a slant path reads

$$I(\rho;z) = W_{xx}(\rho,\rho;z) + W_{yy}(\rho,\rho;z). \tag{22}$$

It should be noted that, in the derivations of Eqs. (18) and (19), we use the following integral and expansion formulas [20–23]:

$$H_n(x) = \sum_{k=0}^{[n/2]}\frac{(-1)^k n!}{k!(n-2k)!}(2x)^{n-2k}, \tag{23}$$

$$\int_{-\infty}^{+\infty} x^n\exp\left[-(x-\beta)^2\right]dx = \sqrt{\pi}(2i)^{-n}H_n(i\beta), \tag{24}$$

$$H_n(x+y) = \left(\frac{1}{2}\right)^{n/2}\sum_{k=0}^{n}\begin{pmatrix} n \\ k \end{pmatrix}H_k\left(\sqrt{2}x\right)H_{n-k}\left(\sqrt{2}y\right), \tag{25}$$

$$\int_{-\infty}^{\infty} H_n(ax)\exp\left[-(x-y)^2\right]dx = \sqrt{\pi}(1-a^2)^{n/2}H_n\left[\frac{ay}{(1-a^2)^{1/2}}\right]. \tag{26}$$

Equations (18–21) are analytical formulas of the PCRPVB through the turbulent atmosphere along a slant path based on the quadratic approximation of the Rytov phase structure function. One can see that the average intensities of PCRPVB in turbulence are mainly determined by the propagation distance z, topological charges l, and zenith angle γ.

3. Numerical Examples and Discussions

In this section, we give some numerical examples to study the average intensity behavior of PCRPVB propagating in non-Kolmogorov atmospheric turbulence along a slant path. To facilitate comparison, we fixed some calculation parameters as follows: $\alpha = 11/3$, $\lambda = 632.8$ nm, $w_0 = 10$ mm, $\delta = 20$ mm, $L = 100$ m, $l = 10$ mm. These values will be used as calculation parameters unless otherwise stated.

First, in Fig. 1, we display the normalized average intensity distribution of PCRPVB with topological charge $l = 3$ emitted at a zenith angle of $9\pi/20$ in non-Kolmogorov atmospheric turbulence at different propagation distances. It can be obviously found that the dark hollow intensity distribution area on the initial plan $z = 0$ of PCRPVB disappears gradually with increase in the propagation distance. In addition, the distribution of the average intensity of PCRPVB remains almost unchanged except that the light spot becomes larger after propagating 8 km ($z > 8$ km). This shows that the intensity of

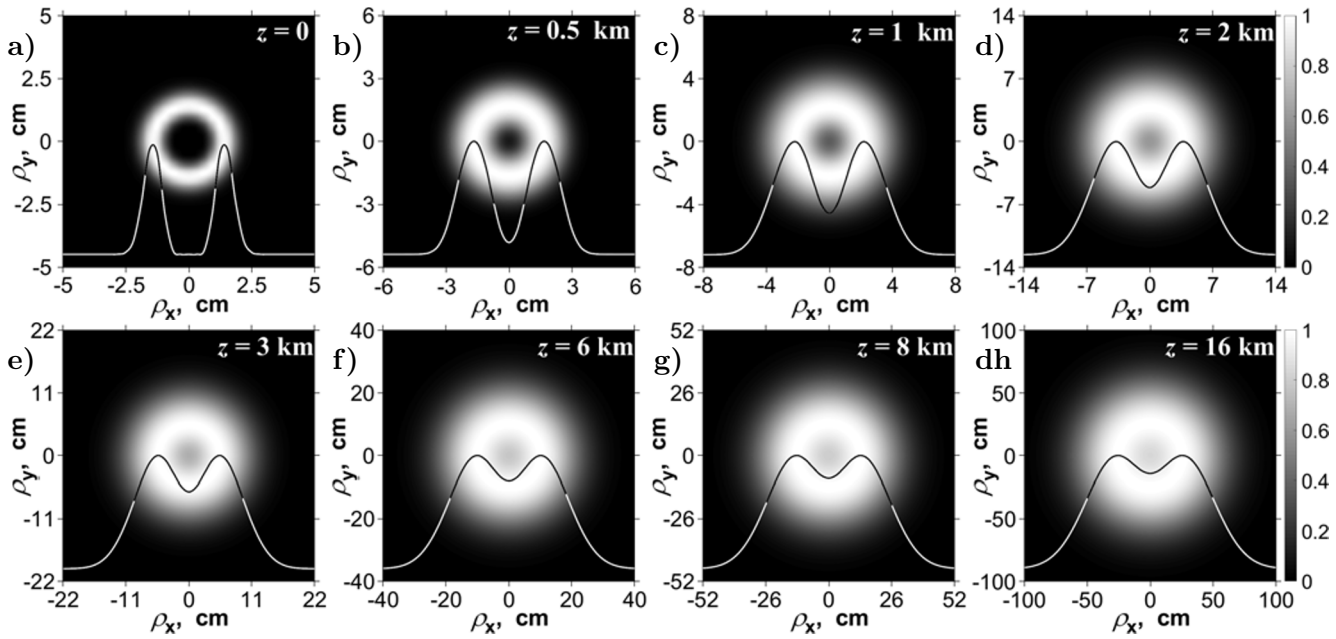

Fig. 1. The normalized average intensity distribution of PCRPVB in non-Kolmogorov atmospheric turbulence along a slant path at different propagation distancel here, $l = 3$ and $\gamma = 9\pi/20$.

atmospheric turbulence at this time is very weak, which can hardly damage the coherence and phase structure of the PCRPVB, so that the intensity distribution of PCRPVB remains unchanged and does not change into a Gaussian-like distribution even after propagating 16 km; see Fig. 1 h. Indeed, when the beam emitted at a zenith angle of $9\pi/20$ propagates 8 km, the actual climbing height of the beam is about 1250 m. According to Eq. (10), the refractive-index structure constant of atmospheric turbulence at this height is $1.173 \cdot 10^{-16}$ m$^{-2/3}$, which belongs to extremely weak turbulence.

In Fig. 2, we show the results of calculations of the normalized average intensity distribution of PCRPVB with topological charge $l = 0$, i.e., partially-coherent radially-polarized (PCRPB)] emitted at different zenith angles in atmospheric turbulence after propagating 3 km. We can see that the hollow degree (the ratio of the central intensity to the maximum intensity, simplified as degree of hollowness) of the beam and is not equal to zero, becomes large with increase in the zenith angle, and the distributions of the light intensity change from hollow-like distribution to Gaussian-like distribution. When the zenith angle is $14\pi/30$, the intensity distribution of PCRPVB almost presents a flat-top beam distribution; see Fig. 2 f, and the beam has become Gaussian-like distribution; see Fig. 2 g, when the zenith angle is $49\pi/100$.

In Fig. 3, we show the normalized average intensity distribution of PCRPVB with topological charge $l = 3$ emitted at different zenith angles in atmospheric turbulence after propagating 6 km. Compared with Fig. 2, one can obviously find in Fig. 3 that the degree of hollowness of PCRPVB is lower, and the light intensity can maintain a better hollow-like beam distribution at a smaller zenith angle; see Fig. 3 a–d. When the zenith angle is $49\pi/100$, PCRPB becomes Gaussian-like distribution, while PCRPVB is only in flat-top distribution. However, the PCRPVB evolves into a Gaussian-like distribution when the zenith angle increases to $199\pi/400$; see Fig. 3 g.

For further comparison, the intensity distributions of PCRPVB with relatively high topological

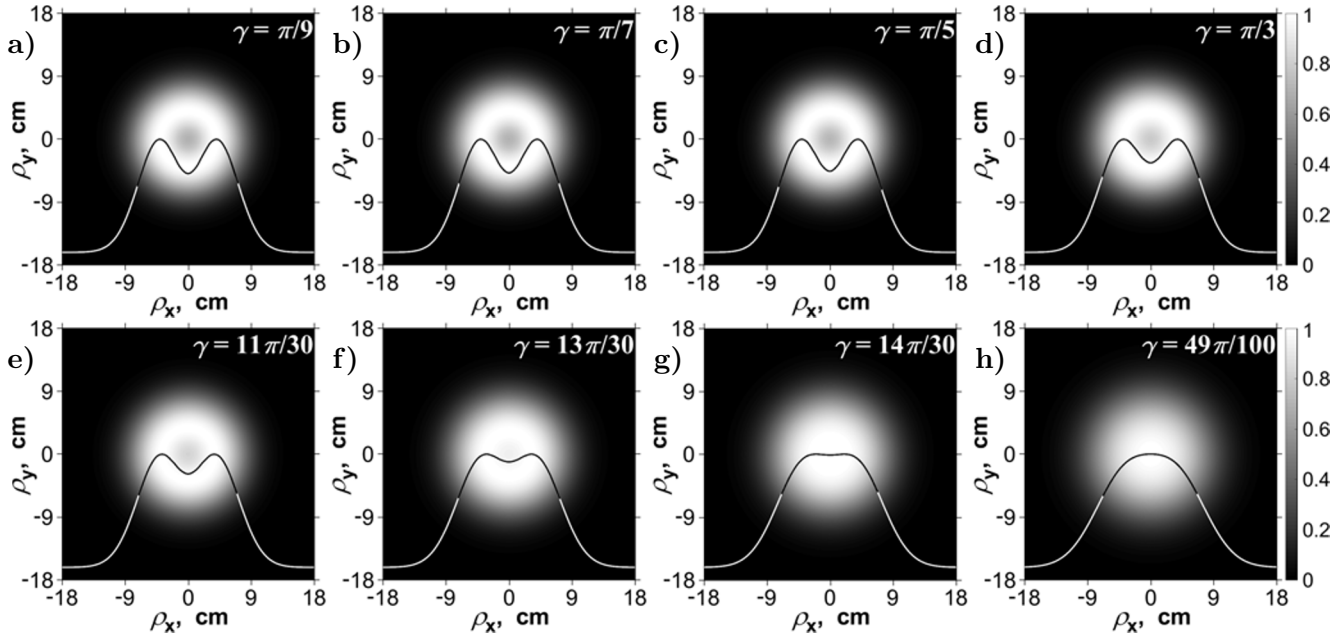

Fig. 2. The normalized average intensity distribution of PCRPVB emitted at different zenith angles in non-Kolmogorov atmospheric turbulence; here, $l = 0$ and $z = 3$ km.

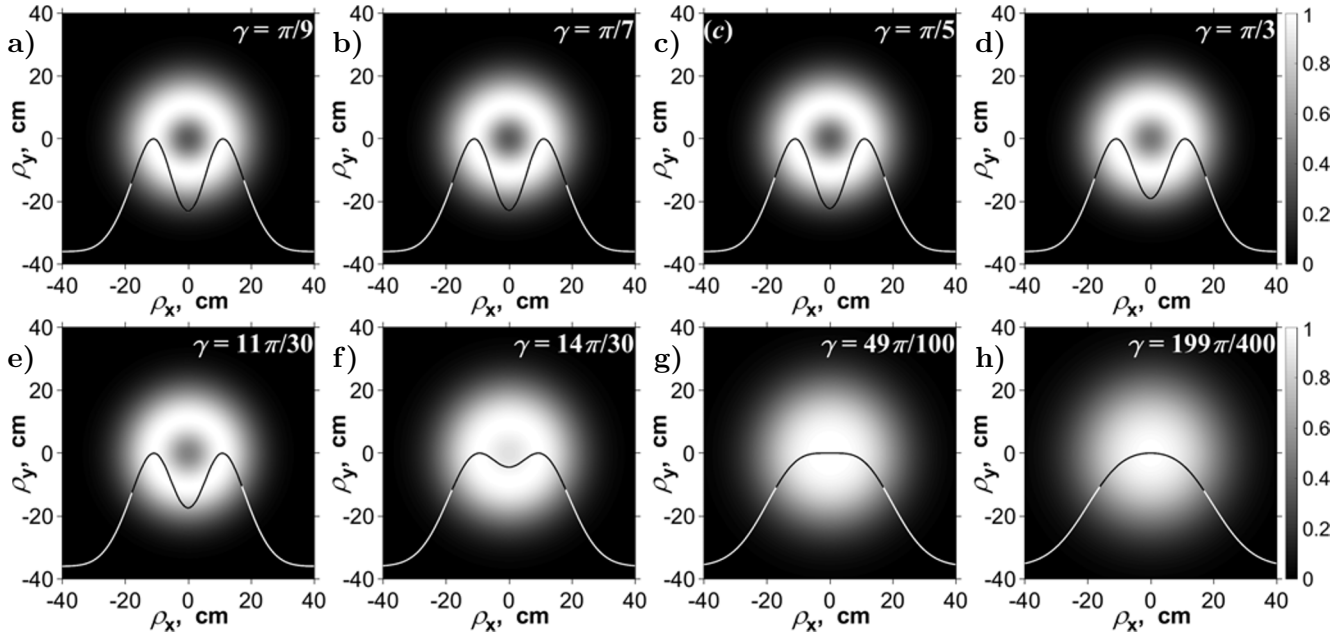

Fig. 3. The normalized average intensity distribution of PCRPVB emitted at different zenith angles in non-Kolmogorov atmospheric turbulence; here, $l = 3$ and $z = 6$ km.

charges l emitted at different zenith angles in atmospheric turbulence are shown in Fig. 4, where the topological charge l is 5 and the propagation distance is 10 km. One can see in Fig. 4 a–d that even though PCRPVB propagates for 10 km at this time, the degree of hollowness of the beam almost ap-

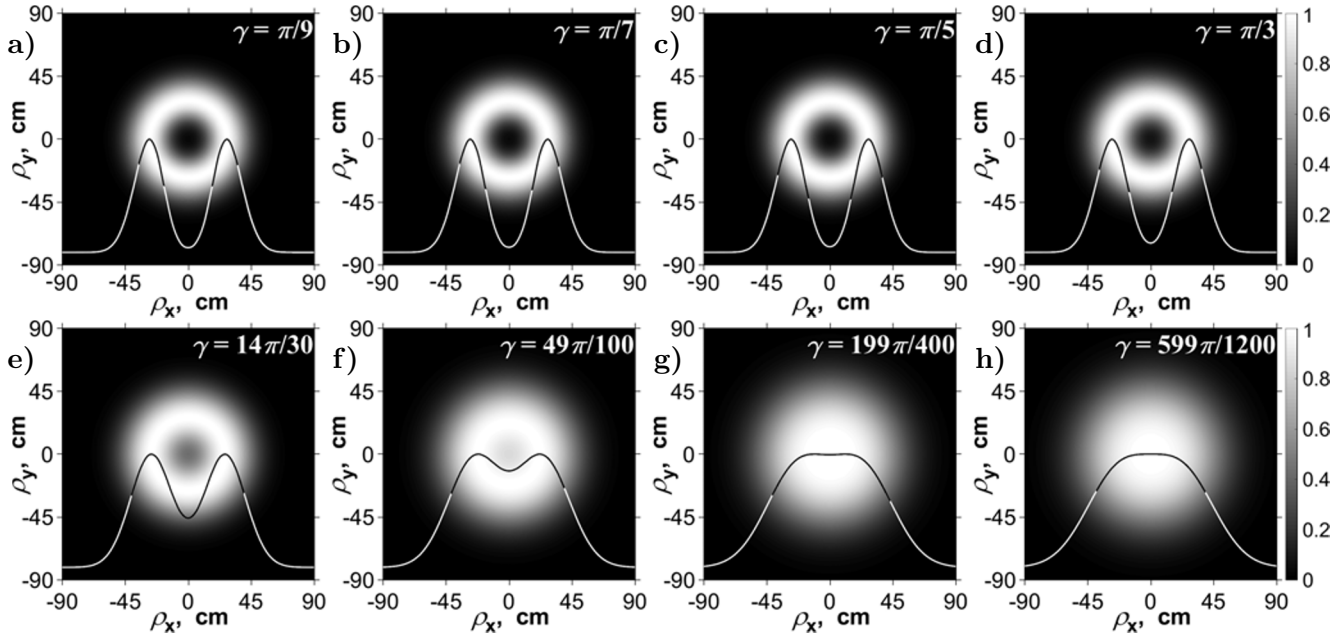

Fig. 4. The normalized average intensity distribution of PCRPVB emitted at different zenith angles in non-Kolmogorov atmospheric turbulence; here $l = 5$ and $z = 10$ km.

proaches 0, and the beam still maintains a hollow distribution. Compared with PCRPVB with $l = 3$, the zenith angle of PCRPVB with $l = 5$ in the flat-top distribution increases from $49\pi/100$ to $199\pi/400$, and the zenith angle of the beam with Gaussian-like distribution increases from $199\pi/400$ to $599\pi/1200$; see Fig. 4 g and h, indicating the PCRPVB with the high topological charges l has the stronger ability of resisting turbulence.

One can see in Figs. 2–4, that PCRPVB (or PCRPB) in atmospheric turbulence is less affected when zenith angle is $[0, \pi/3]$; however, the beam is more affected by zenith angle in the range of $[\pi/3, \pi/2]$. In combination with Fig. 1, one can find that the beam emitted at a small zenith angle is almost difficult to change into a Gaussian distribution unless the beam is kept at a large emission zenith angle. Even for PCRPVB with a high topological charge l, to change into a Gaussian distribution in the end, the emission zenith angle almost approaches to $\pi/2$ (almost parallel to the ground), and a relatively long transmission distance is needed. According to Eq. (10), we can know that atmospheric turbulence intensity decreases rapidly with increase in the ground clearance. This indicates that PCRPVB with high topological charge l shows a very strong ability to resist the interference of atmospheric turbulence. Also, PCRPVB with high topological charge l emitted at the zenith angle in the range of $[0, \pi/3]$ can keep the hollow distribution even after a long propagation distance. Therefore, the use of PCRPVB with high topological charge l is of great significance in many practical applications.

In Fig. 5, we demonstrate the 3D normalized average intensities of PCRPVB in non-Kolmogorov atmospheric turbulence along a slant path for the different zenith angles γ and topological charges l. One finds that PCRPVB with a smaller topological charge $l = 2$ in turbulence gradually evolves into the Gaussian-like beam profile. However, the degree of hollowness of PCRPVB with a larger topological charges $l = 5$ is lower, and the light intensity can maintain a better hollow-like beam distribution at a smaller zenith angle.

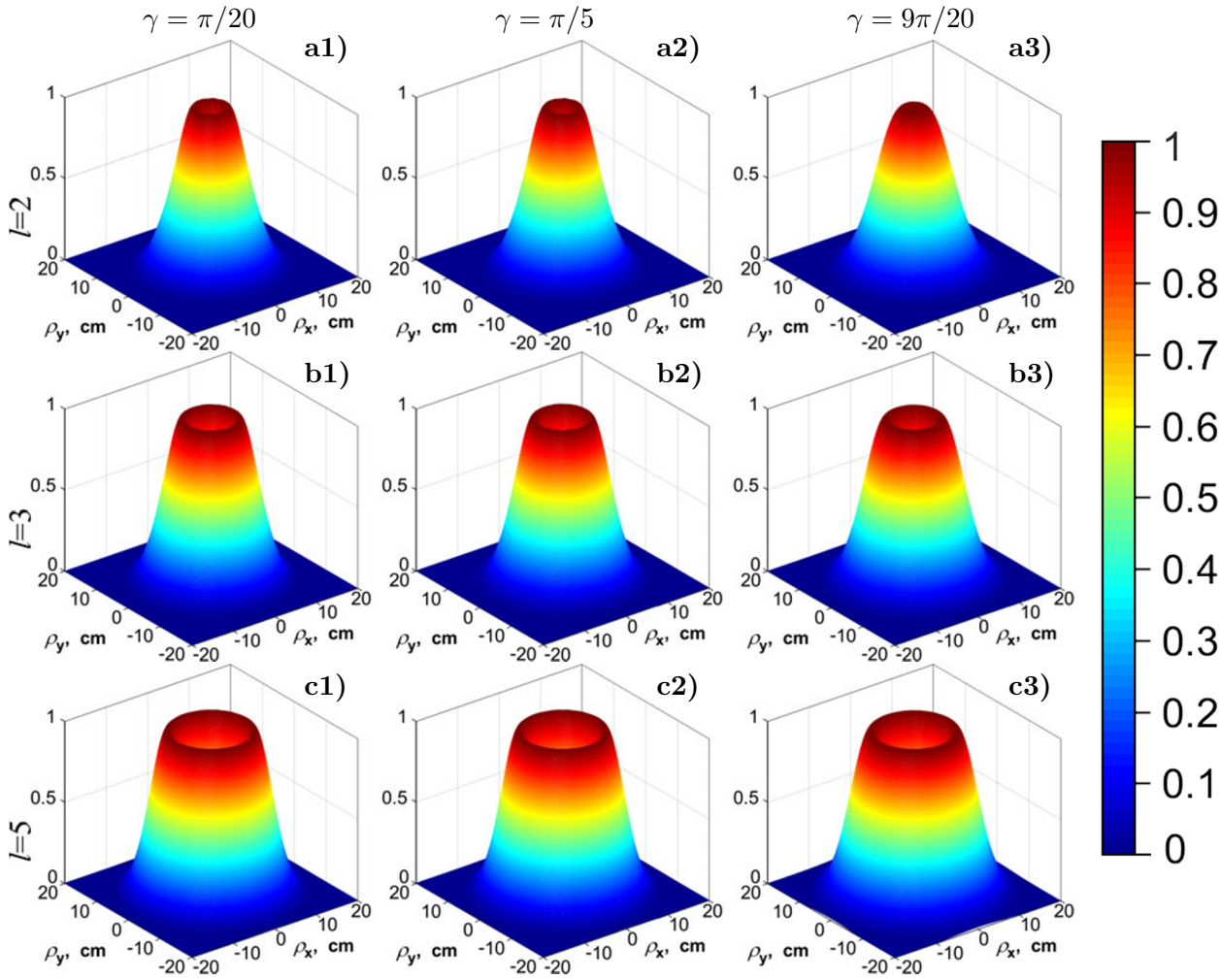

Fig. 5. The 3D normalized average intensity of PCRPVB in non-Kolmogorov atmospheric turbulence for the different zenith angles γ and topological charges l; here, $z = 3$ km.

4. Summary

In this study, we derived the analytical expressions of average intensity of PCRPVB through atmospheric turbulence along a slant path. We studied the effects of topological charge l and emission zenith angle γ on the evolution of beam intensity distribution, giving some numerical examples. The results show that PCRPVB is less affected when zenith angle is $[0, \pi/3]$, and the beam is more affected by zenith angle in the range of $[\pi/3, \pi/2]$. Also PCRPVB emitted at a small zenith angle, in the range of $[0, \pi/3]$, is almost difficult to evolve into a Gaussian distribution. For the PCRPVB to evolve into Gaussian distribution on propagating, it needs a large emission zenith angle and a long propagation distance, and they also increase with increase in topological charge l. Also, we found that PCRPVB with a high topological charge l emitted at a small zenith angle can keep the hollow distribution even after a long propagation distance, $z > 10$ km, which shows a great ability to resist atmospheric turbulence. This is of great significance for many practical applications.

Acknowledgments

The authors acknowledge the financial support provided by the National Natural Science Foundation of China under Grant No. 12033009, the Sichuan Provincial University Key Laboratory of Detection and Application of Space Effect in Southwest Sichuan under Grant No. ZDXM202201003, and the Department of Science and Technology of Sichuan Province under Grant No. 2019YJ0470.

References

1. R. Martinez-Herrero and F. Prado, *Opt. Express*, **23**, 5043 (2015).
2. L. Allen, M. Beijersbergen, R. Spreeuw, and J. Woerdman, *Phys. Rev. A*, **45**, 8185 (1992).
3. S. M. Kim and G. Gbur, *Phys. Rev. A*, **79**, 033844-1 (2009).
4. G. Molina-Terriza, J. P. Torres, and L. Torner, *Nat. Phys.*, **3**, 305 (2007).
5. G. Gibson, J. Courtial, M. Padgett, et al., *Opt. Express*, **12**, 5448 (2004).
6. K. Dholakia and T. Cizmar, *Nat. Photonics*, **5**, 335 (2011).
7. X. Zhang, R. Chen, and A. Wang, *Opt. Commun.*, **414**, 10 (2018).
8. M. Dong, C. Zhao, Y. Cai, and Y. Yang, *Sci. China Phys. Mech.*, **64**, 224201 (2021).
9. J. Shu, Z. Chen, J. Pu, et al., *Opt. Commun.*, **295**, 5 (2013).
10. L. Liu, H. Wang, L. Liu, et al., *Opt. Express*, **30**, 7511 (2022).
11. H. Xu, R. Zhang, Z. Sheng, and J. Qu, *Opt. Commun.*, **480**, 126477 (2021).
12. J. Zeng, C. Liang, H. Wang, et al., *Opt. Express*, **28**, 11493 (2020).
13. Z. Zhou and L. Zhou, *Chinese Phys. B*, **25**, 030701 (2016)
14. H. Xu, R. Zhang, Z. Sheng, and J. Qu, *Opt. Express*, **17**, 23959 (2019).
15. T. Li, M. Sun, J. Song, et al., *Opt. Express*, **29**, 41552 (2021).
16. H. Li, C. Ma, J. Wang, et al., *Opt. Express*, **29**, 39419 (2021).
17. D. Wei, S. Li, J. Zeng, et al., *J. Russ. Laser Res.*, **41**, 364 (2020).
18. J. Li, J. Li, L. Guo, et al., *Waves Random Complex Media*, **31**, 1931 (2021).
19. Y. Xu, Y. Xu, S. Wang, et al., *J. Russ. Laser Res.*, **43**, 509 (2022).
20. J. Yu, Y. Huang, F. Wang, et al., *Opt. Express*, **27**, 26676 (2019).
21. L. Zhao, Y. Xu, N. Yang, et al., *J. Opt. Soc. Am. A Opt. Image Sci. Vis.*, **38**, 1255 (2021).
22. G. Liang, J. Li, Z. Luo, et al., *J. Opt. Soc. Am. A Opt. Image Sci. Vis.*, **36**, 2060 (2019).
23. L. Zhao, Y. Xum and Y. Dan, *Opt. Express*, **29**, 34986 (2021).
24. L. Zhang, D. Deng, X. Chen, et al., *Appl. Phys. B Lasers Opt.*, **125**, 79 (2019).
25. Q. Yang, Y. Gong, Z. Huang, et al., *Appl. Optics*, **59**, 2849 (2020).
26. K. Yong, S. Tang, X. Yang, and R. Zhang, *J. Opt. Soc. Am. B*, **38**, 1510 (2021).
27. Y. Xu, Y. Dan, J. Yu, and Y. Cai, *J. Mod. Opt.*, **63**, 2186 (2016).
28. Y. Xu, T. Yang, Y. Dan, et al., *Optik*, **127**, 7794 (2016).
29. M. Yao, I. Toselli, and O. Korotkova, *Opt. Express*, **22**, 31608 (2014).
30. J. Wang, S. Zhu, H. Wang, et al., *Opt. Express*, **24**, 11626 (2016).
31. T. Yang, Y. Xu, H. Tian, et al., *Optik*, **127**, 10772 (2016).
32. T. Yang, Y. Xu, H. Tian, et al., *J. Opt. Soc. Am. A Opt. Image Sci. Vis.*, **34**, 713 (2017).
33. H. Chen, X. Ji, G. Ji, and H. Zhang, *J. Opt.*, **17**, 085605 (2015).
34. G. Wu, B. Luo, S. Yu, et al., *J. Opt.*, **13**, 035706 (2011).
35. H. Chen, X. Ji, X. Li, et al., *Opt. Laser Technol.*, **71**, 22 (2015).
36. L. Zhao, Y. Xu, and S. Yang, *Optik*, **227**, 166115 (2021).
37. Y. Dan and B. Zhang, *Opt. Lett.*, **34**, 563 (2009).
38. Y. Dan and B. Zhang, *Opt. Express*, **16**, 15563 (2008).